Biomacromolecules

pubs.acs.org/Biomac

Article

Gastropod Slime-Based Gel as an Adjustable Synthetic Model for Human Airway Mucus

Diego Milian, Matthieu Robert de Saint Vincent, Jérémy Patarin, and Hugues Bodiguel*

Cite This: *Biomacromolecules* 2024, 25, 400−412

Read Online

ACCESS | Metrics & More | Article Recommendations | Supporting Information

ABSTRACT: Airway mucus works as a protective barrier in the human body, as it entraps pathogens that will be later cleared from the airways by ciliary transport or by coughing, thus featuring the rheological properties of a highly stretchable gel. Nonetheless, the study of these physical barrier as well as transport properties remains limited due to the restricted and invasive access to lungs and bronchi to retrieve mucus and to the poor repeatability inherent to native mucus samples. To overcome these limits, we report on a biobased synthetic mucus prepared from snail slime and multibranched thiol cross-linker, which are able to establish disulfide bonds, in analogy with the disulfide bonding of mucins, and therefore build viscoelastoplastic hydrogels. The gel macroscopic properties are tuned by modifying the cross-linker and slime concentrations and can quantitatively match those of native sputum from donors with cystic fibrosis (CF) or non-cystic fibrosis bronchiectasis (NCFB) both in the small- and large-deformation regimes. Heterogeneous regimes were locally found in the mucus model by passive microrheology, in which both diffusive and non-diffusive motion are present, similar to what is observed in sputa. The biobased synthetic approach proposed in the present study thus allows to produce, with commercially available components, a promising model to native respiratory mucus regarding both mechanical and, to a lesser extent, physicochemical aspects.

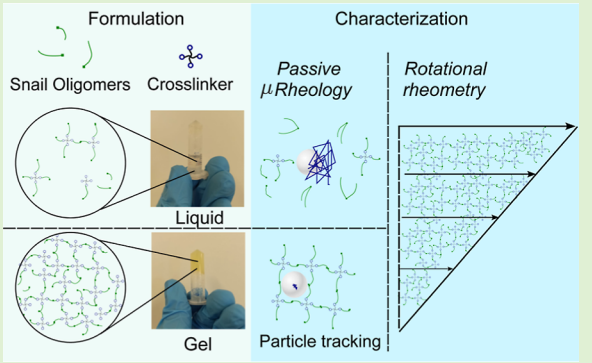

INTRODUCTION

Lung muco-obstructive diseases, such as cystic fibrosis (CF), non-CF bronchiectasis (NCFB), chronic obstructive pulmonary disease (COPD), asthma, among others, have been in the focus of study for many years with the aim of understanding and improving the clearance of respiratory airways.[1] In the healthy state, the mucus is continually secreted and cleared from the airways in a process known as mucociliary clearance. However, under pathological conditions, the clearance becomes less effective, and mucus accumulates in the airways. This accumulation favors inflammation and infection of the airway conducts and in serious cases can lead to permanent loss of pulmonary capacity.

Mucus is a three-dimensional (3D) network composed mainly of water- and gel-forming mucins, which are large glycosylated proteins that associate with each other via disulfide bonds. More complex entanglements also occur as a result of reversible hydrophobic interactions and electrostatic repulsions.[2] This entangled structure gives respiratory mucus mechanical properties characteristic of a viscoelastoplastic gel with large stretchability. However, the fluid mechanics of the transport mechanisms happening within the airway network remains the object of experimental[3,4] as well as numerical[5−7] investigations. Ex vivo samples can be obtained by expectoration when patients are able to produce sputum or more invasively by endotracheal collection,[8] but the availability and reproducibility of samples are not guaranteed, and the collected volumes are very limited (in the order of 10^2 μL or less). In addition, mucus samples collected from patients are often infected or inflamed,[9,10] which makes them unsuitable for in vitro applications where sterile material may be needed. Because of these limitations, there is a great interest in developing a controlled mucus model able to replicate the mechanical properties and physicochemical interactions happening within native mucus.

Exhaustive mucin purification in-lab methods have been published,[11−15] successfully reproducing a gel-like mucus behavior by maintaining its chemical structure, but demanding specific chemistry equipment and access to slaughterhouses (for porcine and bovine mucus), for limited amounts of purified mucins. Conversely, commercially available mucins are easy to obtain but during production they undergo harsh purification processes after which it is difficult to recreate a 3D network by the sample itself.[16−18] The main alterations are the

Received: September 28, 2023
Revised: December 11, 2023
Accepted: December 12, 2023
Published: December 21, 2023

absence of mucins terminal domains, most likely due to protease pepsin digestion,[16] and due to the presence of protein impurities.[13]

Recently, a 3D-mucin network featuring a gel-like behavior has been prepared from bovine and porcine commercial mucins by re-establishing the disulfide bonds thanks to a cross-linker with thiol functional groups.[19,20] The cross-linker consists in a polyethylene glycol core with four arms with thiol groups (hereafter named as PEG-4SH), capable of establishing disulfide bonds. It is recalled that the backbone of the 3Ds structure of mucin networks is given by the multimerization upon the formation of end-to-end disulfide bonds between individual mucin subunits.[21,22] These gels are, however, relatively far from human airway mucus in terms of rheological properties as their storage modulus G' is at least 1 order of magnitude larger than that of pathological mucus.[23,24]

Previous studies on hydrogels with a chemistry based on thiol-ene reactions with PEG-4SH have shown their applicability to the bioengineering field. Such hydrogels have shown good structural and rheological properties to be used as tissue scaffolds,[25] or injectable hydrogels for protein delivery,[26] bone defect repair[27] and bioelectrodes,[28] among other applications. Cytocompatibility and cell viability tests were performed in each study and it was found that such gels are in vivo compatible after analyzing the poor ratio of dead cells by performing live/dead staining[25,27,28] (low cytotoxicity).

Alternatively, approaches including mucins into other gel-forming components have also been proposed. In these formulations, the 3D network is built by alginate gels,[29,30] Carbopol,[31] or locust bean gum.[32] The building blocks for these synthetic 3D networks are jammed configurations, as in Carbopol gels,[33] or cross-links between functional groups or moieties that are not present in native mucus. For example, Carbopol gels are organized in a jammed 3D configuration composed of microsponges[34] that yields at strains in the order of 1−10%,[35] whereas native sputum yields at strains in the order of 10^3%.[24] Therefore, although these formulations provide a relatively good control over the linear rheological properties, they are clearly not representative of the behavior of native sputum at larger deformations, which may be more representative of the efforts involved in cough clearance.[36] Hence the need for a more accurate mucus model to mimic properties not only at rest but also close to its yielding point.

Simultaneously, slime-producing animals such as tadpoles,[37] snails,[38] and hagfish[39] have been gaining attention because of their slimes, which behave mechanically as hydrogels with very large deformability. Particularly, research efforts have enlightened the biochemical and structural composition of snail mucus,[40,41] and it was found that glycoproteins available in these mucus create 3D networks thanks to reversible and irreversible bonds, also found in native mucus (i.e., ion bridges, hydrogen and disulfide bonds[41]). Additionally, snails can be farmed, and stimulated to produce slime on demand, for instance with the cruelty-free Muller method.[42] Snail slime is therefore a more accessible source of mucus than mammal mucus, which is only found in inner organs.

In this study, we investigate the potential of gastropod slime from *Helix aspersa* as a model for airway mucus. Snail slimes are complex mixtures of mainly water (at least 90%[43]), and mucin-like glycoproteins accountable for their viscoelastic character. Other components such as ions, DNA and debris might be found as well.[41] Snail slime has been used and studied historically as a skin care product,[44,45] and more recently because of its adhesive and mechanical properties.[38,46]

With the aid of a thiol cross-linker, we use snail slime to prepare a mucus model with tunable rheological properties. Bulk mechanical properties, and some microstructural properties, are studied by rotational rheometry and passive microrheology, respectively, showing both analogies and differences with human sputum. It is found that cross-linked snail slime is, in regard to its bulk mechanical properties, fairly representative of pathological human sputum, in both small- and large-deformation regimes. Our findings also suggest that the cross-linked snail-slime gel behavior is driven by both the cross-linker and the glycoproteins found in the commercially available snail slime.

MATERIALS AND METHODS

Sample Preparation. *Snail-Slime-Based Gel Preparation.* Snail slime was purchased from Lumacheria Italiana Srl (Cherasco, Italy), obtained from *H. aspersa* adult snails and using the cruelty-free Muller method.[42] The pH of the slime as obtained is about 3.4. The pH of the sample is adjusted to the desired value using a solution of 1 M NaOH (reagent grade, ≥98%, pellets, Sigma-Aldrich, USA) in deionized water. To prepare snail-slime gels, a multibranched cross-linker is added to the slime with variable concentrations (0.5−4 wt %). This cross-linker consists of a 4-arm-polyethylene glycol-thiol molecule (PEG-4SH) with a molecular weight of 10 kDa, purchased from Laysan Bio, Inc. (Tower Drive Arab, Alabama, USA). The cross-linker is dissolved in the slime solution by gentle agitation using a vortex mixer (Stuart SA8, Bibby Sterilin Ltd., UK) at a speed of 250 rpm. Once the sample is homogeneous, it is sealed and put in a thermostatic bath at 37 °C for 4 days. All test were performed after 5 days, once the gelation process has ended and the elastic modulus of the targeted gel remains stable (Supporting Information Figure S1).

Sodium Dodecyl-Sulfate Polyacrylamide Gel Electrophoresis (SDS-PAGE). Samples were denatured with 1× loading buffer at 95 °C for 5 min. A volume of 3−5 μ L of each sample was loaded to gradient SDS-polyacrylamide (BioRad). The gel was migrated at 200 V for 25 min, followed by staining in Coomassie blue and detained in lukewarm water for 30 min. The size of proteins present was compared with the ladder reference.

Collection of Sputum Samples. The complete collection protocol and rheological analysis of sputum samples can be found in a previous publication.[24] Sputum samples were obtained from CF and NCFB patients at the "Centre de Ressource et de Compétence de Mucoviscidose" at Grenoble Alpes University Hospital. All patients included gave their written informed consent, and their clinical information were anonymized and kept confidential. The study was approved by the French research ethics committee (Comité de Protection des Personnes, case number 20.09.08.61213).

Rheology. *Passive Microrheology.* The Brownian motion of particles dispersed in the sample was evaluated through multiple particle tracking. Carboxylated-modified microspheres (FluoSpheres, Invitrogen, Thermo Fisher Scientific, USA), with a nominal diameter of 160 nm (unless otherwise stated), were used as tracers in the snail-slime-based gel and in sputum samples for passive microrheological analysis. For 1 mL of sample, 2 μL of particle solution were added prior to gelation. A volume of 25 μL of sample was placed in a gene frame of 1 cm × 1 cm × 250 μm. Images were obtained using an inverted fast confocal microscope (Nikon Eclipse Ti2) equipped with a fluorescent light source mounted on an epi-fluorescence module. Acquisition was done with a digital CMOS camera (Hamamatsu ORCA-fusion BT) through a 20× water immersion objective. Videos of 10 s length were recorded at a frame rate of 23.3 frames per second (fps) with a resolution of 0.34 μm per pixel. The particle tracking analysis was performed using a customized Matlab script, following the 2D trajectories of individual particles in the horizontal (x, y) plane. For each image frame, the particles were detected according to their intensity weighted by a Gaussian function of the distance from

https://doi.org/10.1021/acs.biomac.3c01043
Biomacromolecules 2024, 25, 400−412

the center. From the recorded individual trajectories, the mean squared displacement (MSD) per particle as a function of lag time (τ) was calculated as $\Delta r^2(\tau) = \langle (r(t+\tau) - r(t))^2 \rangle_t$, where $\langle \cdot \rangle_t$ denotes the time average. The global MSD $\langle \Delta r^2 \rangle$ was calculated by the ensemble averaging of Δr^2.

Verification of Disulfide Bond Network Architecture. As previously introduced, it is known that a fundamental type of bond in mucus architecture is disulfide bond (S−S).[41] To verify that the slime-based gels are also cross-linked by the disulfide bonds, these were targeted using *N*-acetyl cysteine (NAC)-reducing agent. NAC (Viatris, France) was prepared at a concentration of 50 mM, corresponding to one adult dose, and added at a concentration of 5 vol % to a gelled sample. The sample was a snail-slime-based gel prepared with 1.3 wt % of cross-linker and contained carboxylated-modified microspheres of 500 nm of nominal diameter. A blank sample was also prepared by adding 5 vol % of deionized water to compare if there is any dilution effect disrupting the gel. Videos acquired for passive microrheology were performed 5 min after adding either NAC or deionized water.

Oscillatory Rheology. Bulk rheology was evaluated by oscillatory strain sweeps, performed with rotational rheometers Discovery HR-3 (TA Instruments, USA) for the snail-slime-based gels or Rheomuco (Rheonova, France) for native sputa. Two types of geometries were used, depending on the nature of the sample. Gels were analyzed using parallel plate−plate rough geometries (diameter 25 mm), with a gap between the plates ranging from 0.5 to 1 mm, and equipped with a solvent trap when applicable. For nongelled samples, which feature viscosity levels close to that of water, a bob-in-cup geometry was preferred. The cup used had a diameter of 30 mm, and the diameter and length of the bob were 28 and 42 mm, respectively. The gap between the bob and the bottom of the cup was 1 mm.

Strain sweep tests were performed at a constant frequency of 1 Hz in the range of strain increasing from 0.01 to 10,000% at a temperature of 25 °C (37 °C for sputum samples). We verified that the mechanical properties of the snail-slime-based gels were quantitatively comparable at 37 °C (Supporting Information Figure S2). Frequency sweep tests were performed only on gel samples in the range of 0.01 to 10 Hz, at a constant strain of 1%, located in the linear viscoelastic region.

Moreover, as snail slime is secreted by living animals, we also assessed the reproducibility of snail-slime-based gels between batches. The Supporting Information Figure S3 shows that gels from three distinct slime batches, formulated with 1.5 wt % PEG-4SH, are essentially indistinguishable within the measurement uncertainty. This invariance in composition may be due to the fact that each batch pools slime samples produced by large number of animals, thus leveling their individual differences.

Flow Curves. The flow curves of pure snail slime and snail-slime-based gels were obtained by rotational rheometry. Steady-state shear stress was monitored under constant shear rate steps. Once the magnitude of the stress remained constant, its value was taken, and another shear rate step was applied. Shear rates were applied from 100 to 0.1 s^{-1} in decreasing steps. This choice is motivated by the fact that samples slowly evolve, displaying an irreversible transformation under flow representative of a transient state. At low shear rates, this transformation is slow enough to expose the material to solvent evaporation; therefore, the decreasing steps fashion is preferred and no evaporation was observed.

RESULTS AND DISCUSSION

Snail Slime Can Be Cross-Linked by Disulfide Bonds.

Pure snail slime visually presents a yellowish clear liquid aspect. It flows with little apparent resistance under gravity. To give it gel properties, we added a cross-linker (PEG-4SH) in variable concentration and checked, through vial inversion tests (pictures in Figure 1a), whether a gel was effectively formed through its ability to withstand gravity. At its native pH of 3.4, snail slime remains liquid below a concentration of 1.3 wt % of

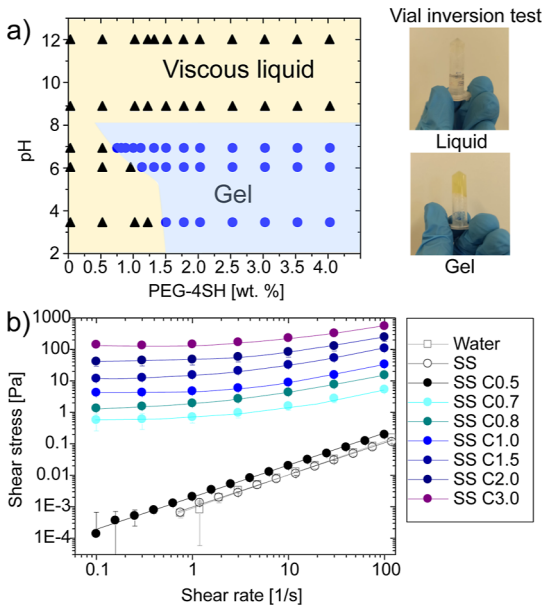

Figure 1. (a) pH-cross-linker concentration phase diagram. Black triangles represent the conditions at which the sample behaves as a liquid, whereas blue circles represent the conditions at which the sample behaves as a gel. The images of the vial inversion test show a sample yielding to gravity ("liquid") and a sample resisting to the effect of gravity ("gel"), respectively. (b) Flow curves of several snail slime (SS) solutions (pH = 7), pure (open circles) and with cross-linker added (filled circles) in increasing concentration (C*x.x*, where *x.x* denotes the cross-linker weight percentage). Water is also depicted for comparison (open squares). Solid lines represent fits to experimental data: linear fits to Newtonian liquids and Herschel−Bulkley fits to gels.

cross-linker, and becomes gelled above. However, while an acidic pH may be representative of the mucus found in the digestive tract, a pH close to neutral would be needed to serve as surrogate in conditions such as those representatives of the airways. We therefore assessed the gelation of snail slime with PEG-4SH under pH conditions ranging from 3.4 to 12 (Figure 1a). In acidic and neutral conditions, the liquid-to-gel transition was found at PEG-4SH concentrations between 0.6 and 1.3 wt %, decreasing when increasing the pH from acidic to neutral.

Contrarily, in alkaline conditions, no gel was produced even when strongly increasing the cross-linker concentration (up to 4 wt %). In previous studies, mucin cross-linking with PEG-4SH had been tested up to 2 wt %.[19,20] It is known that bonds between polysaccharides and peptide cores in mucins are trimmed under alkaline conditions,[47] and that mucin glycoproteins can undergo alkaline hydrolysis.[48] Consequently, the composition of mucins is modified in alkaline conditions and the cross-linker is not able to re-establish disulfide bonds in the trimmed mucin macromolecules.

Snail slime can thus be gelled by adding moderate concentrations of PEG-4SH cross-linker in acidic or neutral conditions. These conditions are representative of various niches in the human body, such as the gastric, intestinal, or airway tracts. As we focus on an airway mucus surrogate, we restrict our characterizations to neutral conditions (pH 7).

The gelation of snail slime by the addition of PEG-4SH was then characterized at neutral pH through flow curves (Figure 1b). Pure snail slime exhibits Newtonian rheological behavior (shear stress is proportional to shear rate within the whole

https://doi.org/10.1021/acs.biomac.3c01043
Biomacromolecules 2024, 25, 400−412

range tested), with a viscosity very close to that of pure water. Adding PEG-4SH in low concentration (0.5 wt %) increases the viscosity by a factor of ∼2, but the solution remains Newtonian. Increasing the PEG-4SH concentration beyond a critical value, $c_0 = (0.6 \pm 0.1)$ wt %, drastically changes the rheological behavior of the mixture, which now features a plateau at low shear rate, followed by a sublinear increase of the shear stress with respect to the shear rate at high rates. This flow behavior is very well adjusted to an Herschel−Bulkley model, $\tau = \tau_y + K\cdot\dot{\gamma}^n$, in which τ is the shear stress, K is the consistency index, $\dot{\gamma}$ is the shear rate and n the flow index, characterizing a viscoelastic shear-thinning material ($0 < n < 1$) with yield stress ($\tau_y \geq 0$). The fits using this model are represented by the solid lines in Figure 1b at concentrations $c > c_0$, and the fitting parameters can be found in the Supporting Information Table S4. It is remarked that the shear thinning index remains almost constant no matter the concentration of cross-linker added in the formulation. The presence of a yield stress indicates that a structural component in the sample makes it behave as an elastic solid at rest,[49] which fades giving place to flow when the sample is stressed beyond the yield stress.

The addition of PEG-4SH in sufficient concentration is thus needed to get a gelled structure, which confirms that snail slime molecules cannot bond by themselves. We hypothesized that this inability to self-bond could be a marker of relatively small slime mucin macromolecules. We therefore analyzed by SDS-PAGE the molecular weight of the snail-slime solution, both pure and with cross-linker added beyond c_0 (Figure 2a).

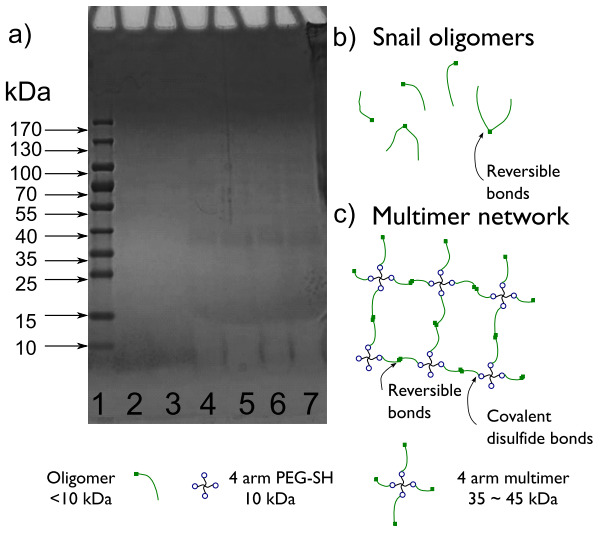

Figure 2. SDS-PAGE of snail-slime-based samples. Lane 1 shows the scale going, from bottom to top, from 10 to 170 kDa, respectively. Lanes 2 and 3 are the result for pure snail-slime samples. Lanes 4 and 5 stand for cross-linked snail slime with 1.3 wt % of PEG-4SH. Lanes 6 and 7 stand for cross-linked snail slime with 2.0 wt % of PEG-4SH.

For pure snail slime (lanes 2 and 3), the sample migrates into the chromatography gel readily, reaching values of molecular weight lower than 10 kDa. This very low value is troubling because native mucins are known to reach weights from 2−50 MDa,[2,16] depending on the purification process. No larger residue was found at the entrance of the chromatography gel, excluding the possibility of larger molecules in the sample. Therefore, the macromolecules present in the snail slime are lighter than 10 kDa and are found like diluted chains, hereafter referred to as oligomers, as presented in Figure 2b. The small size of the objects found for pure slime might explain why the snail slime used in this study does not form a gel by itself, but more analyses are needed to confirm this hypothesis. SDS-PAGE chromatograms on cross-linked gels show a wide band at molecular weights close to 15 kDa (lanes 4−7), and another, very weak, band between 35 and 40 kDa that is slightly more pronounced at higher cross-linker concentration (lanes 6 and 7). Note that the band below 10 kDa found in pure slime has completely vanished, which suggests that there is neither free oligomer or free PEG-4SH left in the gelled samples. The two observed bands suggest that the PEG-4SH molecules bond with respectively one oligomer, leaving them three free arms, or with four, making all possible connections on each cross-linker molecule; the latter configuration increases by increasing the cross-linker concentration as can be inferred by the slightly stronger intensity of the ∼35 kDa band in lanes 6 and 7. The absence of any heavier molecule suggests that the oligomers can only be connected to one single PEG-4SH molecule. The existence of a three-dimensional network, confirmed by the existence of a yield stress, is thus due to reversible end-to-end associations of cross-linked multimers (Figure 2c), which were broken when the sample was injected into the chromatography gel.

To validate the idea that PEG-4SH cross-linking is responsible for the covalent cross-linking of snail slime, we treated gelled samples with *N*-acetylcysteine (NAC), and analyzed their structural response through microrheology. NAC is a commercial mucolytic drug known for specifically breaking disulfide bonds.[50,51] Figure 3 compares the trajectories of tracer particles in a cross-linked sample after addition of 5 vol % of deionized water (control, Figure 3a−c), and 5 vol % of 50 mM NAC (treated, Figure 3d−f). Each individual particle tracked visibly explores a much wider space in the treated sample than that in the control (Figure 3a,d). Quantitatively, the time-dependence of the particle square displacement, $\Delta r^2 \sim \tau^\alpha$, almost flat in the control sample ($\alpha \simeq 0$, Figure 3b), increases up to a close to linear trend ($\alpha \simeq 1$, Figure 3e). This increase is the signature of a transition from an almost purely elastic gel to a viscoelastic fluid. The mean square displacement also increases by 3 orders of magnitude (Figure 3c,f), corresponding to a similar decrease of the viscoelastic modulus. Taken together, these data confirm that the disulfide bonds formed by the addition of PEG-4SH are the origin of the main backbone of the gelled structure of snail-slime-based gels.

Time- and Shear-Sensitivity of Snail-Slime-Based Gel. The rheological behavior of cross-linked snail slime is analyzed in oscillatory rheology. Strain sweep (Figure 4a) shows a wide linear viscoelastic region in which both G' and G'' remain constant regardless of the strain applied. In this region, G' is higher than G'' indicating gel behavior. This gel behavior is confirmed in the frequency range between 0.01 and 10 Hz (Figure 4b), scoring that the cross-linked slime does not flow even in time scales of minutes. In addition, a relaxation of the network is not expected as the structure of the gel is covalently bonded by the cross-linker, and therefore a moduli crossover is not foreseen with this configuration (moduli slope ∼0). Out of the linear domain in the strain sweep, when strain increases up to values higher than ∼1000%, the G' curve drastically decreases and crosses the G'' curve. Beyond this crossover point, defined as $\gamma = \gamma_c$, the sample's response is dominated by

https://doi.org/10.1021/acs.biomac.3c01043
Biomacromolecules 2024, 25, 400−412

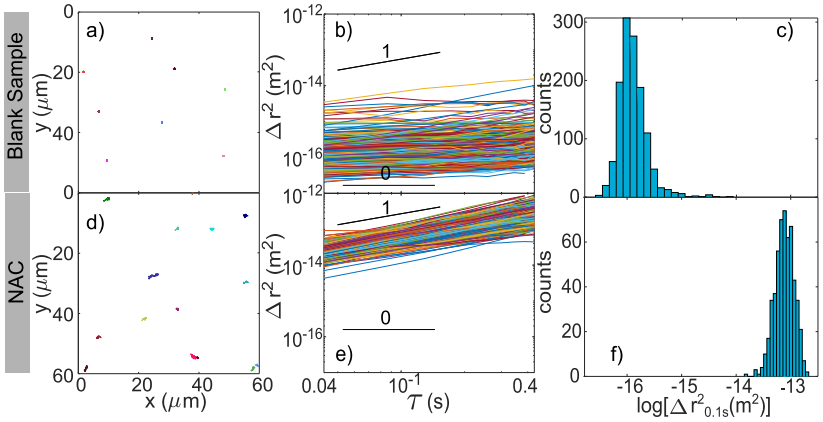

Figure 3. Microrheological results for a snail-slime-based gel (1.3 wt % cross-linker) under different treatments. Tracers are carboxylated-modified microspheres of 500 nm diameter. The blank sample corresponds to the addition of 5 vol % of deionized water onto the gel. The NAC treatment corresponds to the addition of 5 vol % of 50 mM NAC onto the gel. (a,d) display the trajectories of particles in a cropped frame of the image. (b,e) display the individual square displacement Δr^2 as a function of the lag time τ. (c,f) display the distribution of $\log(\Delta r^2)$ at a fixed lag time of 0.1 s.

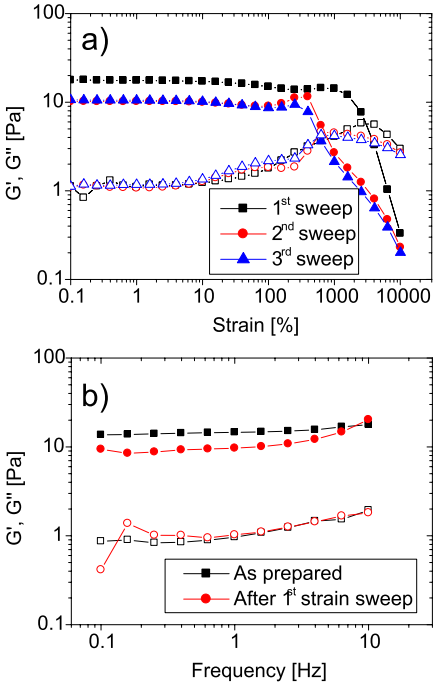

Figure 4. Rheological behavior of a snail-slime-based gel (1.3 wt % cross-linker); filled and open symbols denote the storage (G') and loss (G'') moduli, respectively. (a) Strain sweep performed at 1 Hz; three consecutive tests are represented. (b) Frequency sweep performed at 1% strain, before and after a strain sweep test.

energy dissipation. Structurally, the sample loses part of its initial microstructural organization and starts to flow. Cross-linked snail slime thus behaves as a viscoelastoplastic fluid with a large ability to deform before flowing.

To check if the gelled structure reforms after flowing, consecutive strain sweeps were performed on a single sample. We analyze if the gel sample could recover its solid-like behavior after having withstood efforts beyond its critical strain γ_c. Figure 4 also shows the response of the same snail-slime-based gel sample after up to three consecutive strain sweeps, each being followed by a time sweep at 1% strain for 1000 s (data not shown).

After the first strain sweep, we observe that G' immediately recovers and keeps a value higher than G'' throughout the first time sweep. The sample therefore recovers its solid-like behavior immediately after the cessation of flow (data not shown). This immediacy indicates that the gel viscoelastic properties are time-independent: any material relaxation would happen on a time scale much shorter than ∼1 s. Then, the second strain sweep features a rheological response qualitatively similar to that of the sample as prepared (Figure 4a). Quantitatively, the linear elastic response of the sheared gel drops by a factor of ∼1.7 compared to its original value; the viscous response does not evolve substantially. Similar evolution can also be observed when comparing the frequency response of the sample before and after a strain sweep was applied (Figure 4b). This reduction on G' is more pronounced on gels prepared with cross-linker concentrations below 2.0 wt % PEG-4SH, and becomes marginal, in order of a few percents or less, at higher cross-linker concentrations. The first strain sweep also affects the crossover point, reducing both the critical deformation γ_c by almost 1 order of magnitude, and the critical stress, $\sigma_c = \sqrt{G_c'^2 + G_c''^2}\,\gamma_c$ where $G_c' = G_c''$ is the modulus at crossover, by a factor of ∼5.3.

Once the gel underwent the first set of strain and time sweeps, the same test is repeated up to three times. It is observed that neither the linear nor the crossover properties evolve significantly after these consecutive tests. Therefore, after the material has been sheared once beyond its crossover point, it attains a new structural state, with slightly degraded elastic properties, that can withstand shearing without undergoing further transformation. The first strain sweep thus acts as a preshear of the gel which then reaches a stable structure that persists under the following strain and time sweeps. In the following, all characterizations will be performed on presheared samples, unless otherwise stated.

Comparison to Human Sputum: Similarities and Differences. The objective of the present study is to formulate a biobased material that mimics the rheology of human respiratory mucus. Figure 5 compares the rheological responses of a snail-slime-based gel (1.3 wt % PEG-4SH) to two sputum samples obtained from distinct patients with NCFB. The same qualitative behavior is retrieved in the three samples: a wide linear viscoelastic domain characterized by a plateau with $G' > G''$, followed by a relatively abrupt decrease of G' that intersects G''. In addition, the frequency behavior of sputum samples, as reported e.g. in Tomaiuolo et al.[9] for CF

https://doi.org/10.1021/acs.biomac.3c01043
Biomacromolecules 2024, 25, 400−412

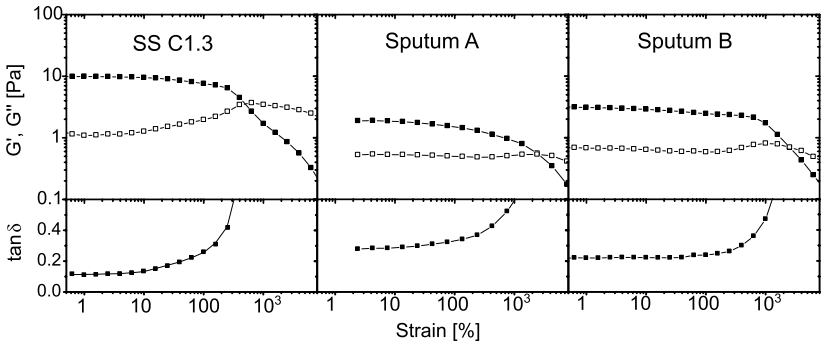

Figure 5. Rheological comparison between a slime-based gel (1.3 wt % PEG-4SH) and two sputum samples from patients with non-CF bronchiectasis (NCFB). Filled and open symbols represent G' and G'', respectively.

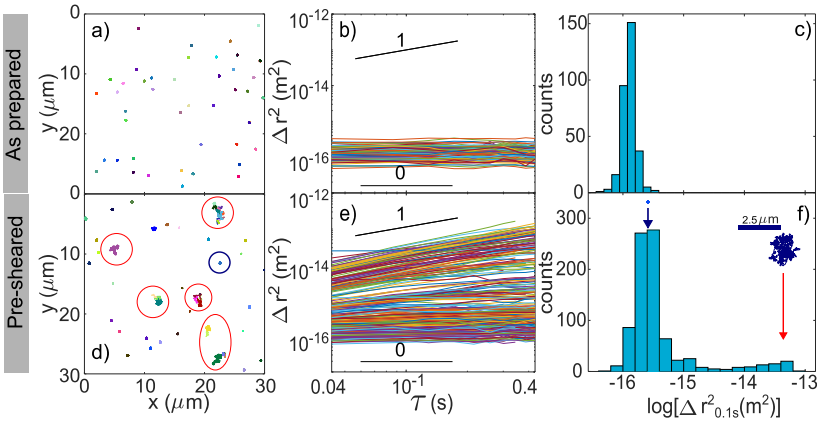

Figure 6. Microrheological results for a snail-slime-based gel (1.3 wt % cross-linker), as prepared (a,c) and presheared (d–f). Tracers are carboxylated-modified microspheres of 160 nm diameter. (a,d) display the trajectories of particles in a cropped frame of the image. (b,e) display the mean square displacement Δr^2 as a function of the lag time τ. (c,f) display the distribution of $\log(\Delta r^2)$ at a fixed lag time of 0.1 s. The red circles in (d) highlight the abnormally mobile particles visible in the frame; the blue circle denotes a typical particle. An example of particle trajectories is shown in (f) for diffusive (abnormally mobile, red arrow) and non diffusive (blue arrow) motion.

sputum, and for Patarin et al.[23] for CF and COPD sputum, is also qualitatively similar to that of snail-slime-based gels. Quantitatively, the linear elastic and viscous moduli of the slime-based gel sample are higher than those of the two sputum samples (respectively, G' = 10, 2, and 3 Pa, and G'' = 1, 0.5, and 0.7 Pa), and the damping ratio $\tan\delta = G''/G'$ is accordingly much lower in the slime-based gel than in the sputa (0.1 vs 0.2–0.3). The crossover point for the slime-based gel sample is found at $\gamma_c \simeq 500\%$, smaller than that of the two sputum samples, $\gamma_c \simeq 2000\%$. These values indicate that although both systems share a similar gel behavior, the slime-based gel model is, at this PEG-4SH concentration, stiffer and less dissipative than human respiratory mucus.

Another structural difference can be inferred from a closer inspection of the strain sweep curves in the intermediate deformation range, between ∼10% and γ_c. In the slime-based gel, the G'' curve substantially increases before it intersects with G'; correspondingly, the damping ratio increases sharply. In contrast, sputum sample A features an almost flat G'' curve up to γ_c, and the gradual increase of $\tan\delta$ is rather due to the gradual decrease of G'. Nevertheless, several samples, such as sample B in Figure 5, also present a clear increase of G'' before the crossover point, yet to a lesser extent than observed (systematically) in the slime-based gel. This behavior was observed in 38% of the samples from the CF cohort (N = 13) and in 50% of the samples belonging to the NCFB cohort (N = 10).

The G'' overshoot corresponds to a so-called Type III complex fluid in a classification proposed by Hyun et al.[52] An example of a material found in this classification is Xanthan Gum, in which the G'' overshoot is argued to originate from the resistance of a complex structure toward strain. Consequently, the G'' overshoot is believed to originate from large scale rearrangements or side chain interactions. A recent study has elucidated that the G'' overshoot is not only due to a transient state between the strain that is dissipated and stored, but mostly to a heterogeneous propagation of the yielding within the structure of the material.[53]

To retrieve these structural differences, we analyzed the samples with microrheology. The slime-based gel was first analyzed as prepared, i.e. without prior preshearing (Figure 6a–c). Tracer particles feature very low mobility, as expected from a mostly elastic gel, with particle square displacement values tightly distributed around 1×10^{-16} m^2. As the slope of Δr^2 as a function of lag time τ is close to 0, it is possible to assert that the mean square displacement of particles is independent of the lag time. It is therefore possible to estimate $G' \simeq \frac{2k_BT}{3\pi a\langle\Delta r^2\rangle}$, with k_BT the thermal energy and a the particle radius, resulting in an elastic modulus of 6.1 Pa, in order-of-magnitude agreement with the macroscopic value before preshearing (G' = 17.5 Pa). Previous studies on mucus surrogates show results from rotational rheometry and passive microrheology for cross-linked commercial mucins using PEG-

https://doi.org/10.1021/acs.biomac.3c01043
Biomacromolecules 2024, 25, 400–412

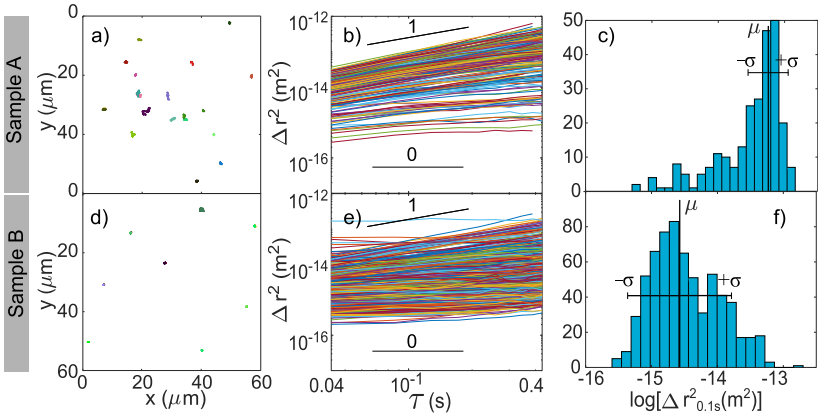

Figure 7. Microrheological results for the sputum samples A and B are represented in Figure 5. Tracers are carboxylated-modified microspheres of 160 nm diameter. (a,d) display the trajectories of particles in a cropped frame of the image. (b,e) display the mean square displacement Δr^2 as a function of the lag time τ. (c,f) display the distribution of $\log(\Delta r^2)$ at a fixed lag time of 0.1 s. The mean μ and standard deviation σ are calculated from the logarithmic values of Δr^2.

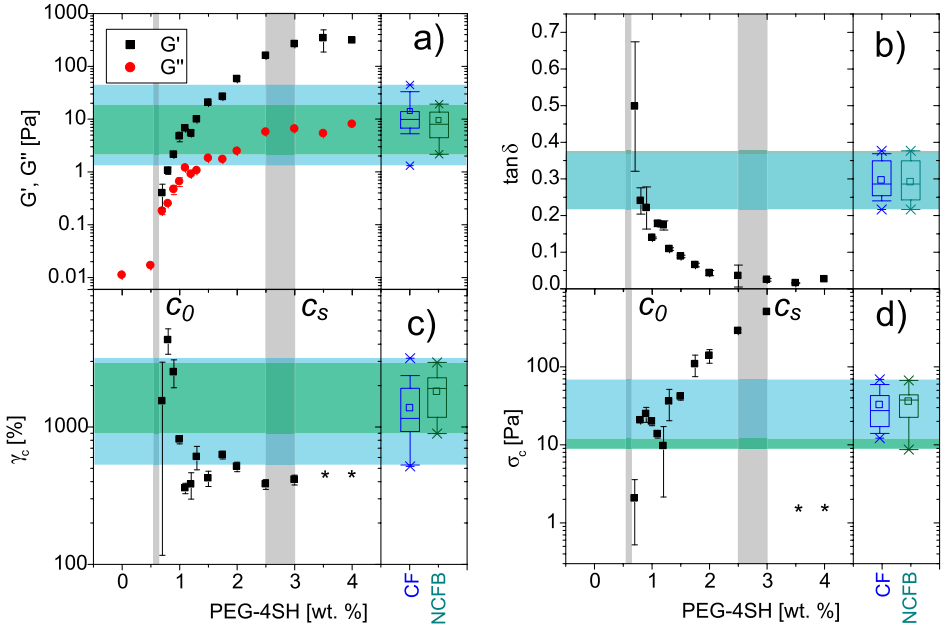

Figure 8. Evolution of the slime gel rheological properties with cross-linker concentration. (a) Linear elastic and viscous moduli G' and G''; below c_0, G' was not measurable. (b) Linear damping ratio tan δ. (c) Critical deformation γ_c. (d) Critical stress σ_c. Stars (*) denote samples on which the crossover point could not be determined because samples had been out of the shearing geometry before the crossover point was reached. For each cross-linker concentration, at least 2 replicates were tested; data points and error bars denote the mean and standard deviation, respectively. The distribution of rheological values in CF and NCFB sputa is also indicated as box and whiskers for comparison (N = 13 and 10, respectively); the blue and green shaded areas represent the corresponding spanning ranges. The light gray areas represent the estimated gel point and saturation concentrations, c_0 and c_s, respectively.

4SH. For these samples, the value of $\langle \Delta r^2 \rangle$ is reported and can be used to estimate and compare G' as done herein to the value obtained macroscopically in the linear regime. It is found that microrheological values are systematically smaller than macrorheological ones by up to 2 orders of magnitude.[19,20] In comparison, we show that the probes used to study the local properties of the snail-slime-based gel network at the microscale are able to describe the macroscopic behavior in agreement with the order of magnitude (a factor of ~3 for G').

The sharp distribution of Δr^2 indicates that the unsheared material is spatially homogeneous. However, after preshearing (Figure 6d–f), the mobility of most tracer particles slightly increased, but most importantly, several tracers (examples visible in Figure 6d are circled in red) were found abnormally mobile, almost purely diffusive ($\alpha \rightarrow 1$), with individual square displacement values increased by up to 3 orders of magnitude (see the secondary peak in Figure 6f). The observation of this highly mobile particles subpopulation strongly suggests that the preshear created heterogeneous yielded zones in the material, in agreement with the rheological observation and the interpretation of a G'' overshoot.

Accordingly, the microrheological behavior of sputum samples A and B is displayed in Figure 7. Sample A (Figure 7a–c) shows a predominant diffusive behavior compared to sample B (Figure 7d–f), showing both diffusive and non-diffusive behaviors. Sample A is also more dissipative and more homogeneous, as highlighted by the higher average (μ) and lower dispersion (σ) of Δr^2 compared to sample B.

https://doi.org/10.1021/acs.biomac.3c01043
Biomacromolecules 2024, 25, 400–412

Schematically, sputum A is predominantly homogeneous and diffusive, whereas sputum B is rather heterogeneous and weakly diffusive.

This distinction is, at first sight, rather surprising because sputum samples A and B are closely comparable on the macroscopic scale (Figure 5). However, the more diffusive behavior observed in sample A is in agreement with its higher value of tan δ. The observation of a G'' overshoot in sputum sample B, yet not as pronounced as in the snail-slime-based gel, is also consistent with its higher microscopic heterogeneity, following the idea that the overshoot originates from the uneven distribution of the strain within the sample.[53] The slime-based gel thus mimics, and even exacerbates, the heterogeneous yielding propagation observed in a substantial minority of sputum samples (43% of the present cohort).

In summary, cross-linking snail slime with PEG-4SH allows to produce gels with viscoelastoplastic behavior. Structurally, these samples are much less dissipative than human respiratory mucus and tend to yield in preferential zones, which is not usual in sputa. Their main macrorheological characteristics are nevertheless similar, in order of magnitude, to those of human sputa. Since PEG-4SH drives the gelation, a closer match of these rheological properties can be expected by adjusting the cross-linker concentration.

Snail-Slime-Based Gels are Rheologically Tunable. At given pH, varying the cross-linker concentration affects the rheological properties, as we observe a sharp transition from a viscous liquid to gel behavior (Figure 1b). Beyond this transition, the rheological curves in strain sweep remain qualitatively similar to Figure 4a, allowing us to define five representative parameters: the elastic and viscous moduli G' and G'' and the damping ratio tan δ, taken in the linear viscoelastic regime at 1% deformation; the crossover strain γ_c and stress σ_c. The evolution of these parameters with the cross-linker concentration is represented in Figure 8.

As anticipated from the flow curves (Figure 1b), the strain sweep data confirm that concentrations of cross-linker lower than 0.6 wt % do not confer the sample any gel character. In the linear regime, G' was not measurable, and no crossover was found; G'' is in the order of 10^{-2} Pa, in close agreement with the viscosity deduced from flow curves. In the gel domain (cross-linker concentration of 0.6 wt % or above), G' becomes larger than G'' and both increase abruptly compared to the liquid regime, starting respectively at values of 0.4 and 0.2 Pa (Figure 8a). The moduli then rapidly increase with concentration, gaining respectively a factor of ∼750 (0.4−300 Pa) and ∼40 (0.2−8 Pa). In terms of linear viscoelasticity, slime-based gels can thus reproduce sputa in cross-linker concentrations below 2%. The evolution of elastic and viscous moduli then saturates at crossover concentrations beyond $c_s \simeq$ 2.5−3 wt %. This slowing down of the hardening trend may indicate that cross-linker has saturated all binding sites to continue building a harder network.

Due to the critical nature of the sol−gel transition, rheological and dynamic properties exhibit scaling behavior close to the gel point c_0.[54] In particular, the viscoelastic modulus $G^* = \sqrt{G'^2 + G''2}$ follows $G^* \propto (p - p_c)^z$, where p is the link density and p_c the critical one at which an infinite cluster is formed. Assuming that the link density is proportional to the cross-linker concentration c, we should expect that $G^* \propto (c - c_0)^z$. This hypothesis is tested in Figure 9. Not only the elastic modulus but also the yield stress τ_y and the stress at

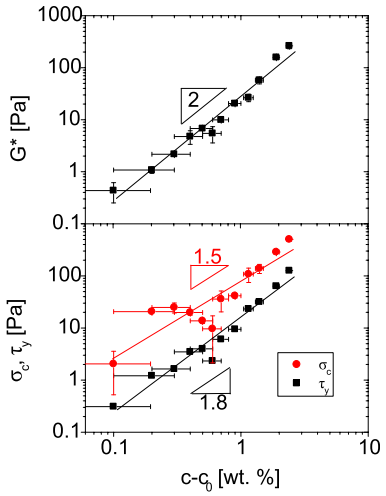

Figure 9. Evolution of (a) the viscoelastic modulus G^* and (b) the critical and yield stresses, σ_c and τ_y, with the excess PEG-4SH concentration above gelation, $c - c_0$, excluding the data above the saturation concentration ($c_s \simeq$ 2.5−3 wt %). Solid lines represent power law fits to the experimental data. The power index of the fit is given for each curve.

the crossover σ_c indeed follow a power relation with respect to $(c - c_0)$ with an exponent z of about 2. Percolation theory in the Zimm−Rouse limit predicts $z = 8/3$,[55] electrical analogy predicts $z = 1.94$,[56] while experimental results lie in the range 1.5−3 depending on the systems.[57−60] This critical behavior in the vicinity of the gel point confirms that the cross-linker concentration controls the density of links in this regime. However, when increasing the cross-linker concentration further, and above c_s, the maximum possible number of cross-links is reached and the elastic modulus saturates.

As G' increases faster than G'' with the cross-linker concentration, the value of tan δ sharply decreases, before stabilizing beyond ∼2.5 wt % (Figure 8b) at very low values within 0.015−0.025. This behavior indicates that the dissipative share of the material rapidly decreases as the density of cross-links increases, exhibiting a very strong solid-like behavior. Thus, the concentration ranges which allow mimicking sputum is narrow, between 0.7 and 0.9 wt %.

Outside of the linear domain, the critical deformation γ_c and stress σ_c feature contrasted evolutions (Figure 8c,d). The critical deformation γ_c sharply decreases as the cross-linker concentration increases up to 1.5 wt % (Figure 8c). This is consistent with the fact that the elastic behavior of the samples become more predominant over viscous when increasing the cross-linking in gels, tending to produce a more robust material, but as a counterpart that starts to flow at lower strains. At higher crossover concentrations, γ_c stabilizes around about 400%, slightly below the typical range for sputum. Note that it was not possible to obtain reliable information for cross-linker concentrations ≥3.5 wt %, because the samples get out of geometry before reaching the crossover point as a consequence of their elasticity generating a difference in normal forces.[61]

Lastly, the critical stress σ_c tends to increase with the cross-linker concentration in the gel regime, even when the critical deformation has leveled up. However, the increase in σ_c follows the same trend as G' as a function of concentration, but as we lack experimental data at concentrations of cross-linker ≥3.5 wt %, it is not possible to see a stabilization of its value as

https://doi.org/10.1021/acs.biomac.3c01043
Biomacromolecules 2024, 25, 400−412

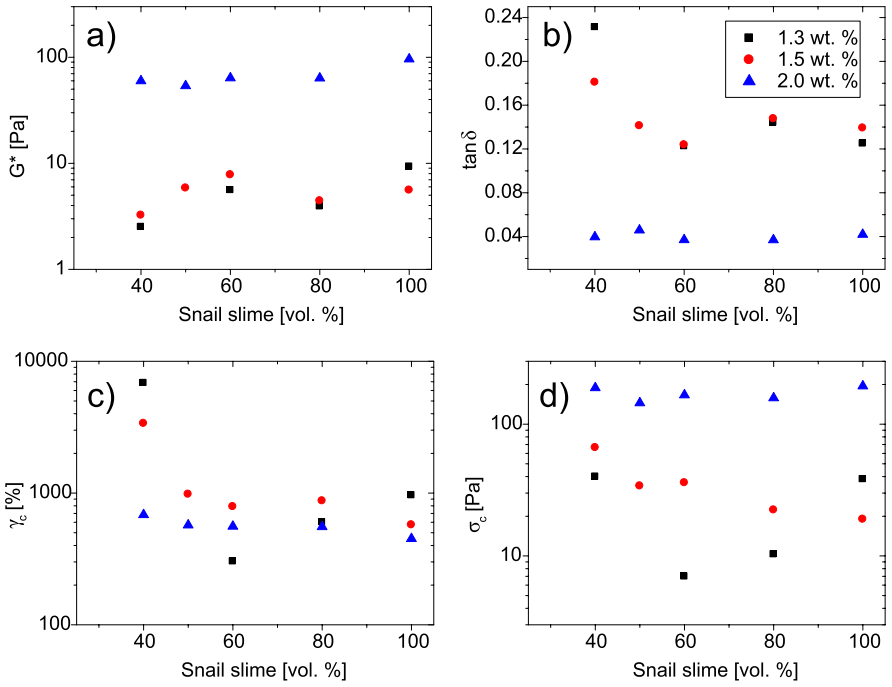

Figure 10. Evolution of the gel rheological properties with snail slime dilution. (a) Linear viscoelastic modulus G^*, (b) linear damping ratio tan δ, (c) critical deformation γ_c and (d) critical stress σ_c. Black squares, red circles and blue triangles correspond to cross-linker concentrations of 1.3, 1.5, and 2.0 wt %, respectively.

observed with G'. In the tested concentration range, σ_c values span from 2 to 500 Pa, and can be representative of pathological sputum between 0.8 and 1.5 wt % cross-linker.

In summary, adjusting the cross-linker concentration allows tuning of the rheological properties of slime gels and reproduction of at least one of the main rheological parameters (linear viscoelasticity, damping ratio, critical strain, and stress) of representative pathological sputum. A narrow concentration range, between 0.8 and 0.9 wt % cross-linker, even matches the four rheological parameters together. These snail-sludge-based gels can therefore be considered as suitable rheological models of human CF or NCFB sputum.

Another way of adjusting the gel rheological properties is through the slime concentration, which can be achieved by diluting the commercial solution. For this purpose, the slime is diluted with distilled water before adding the cross-linker. Figure 10 shows how slime dilution, represented here as the volume fraction of the mother slime solution relative to the total volume, affects each of the rheological markers considered. Note that no gel was formed below 40 vol % slime. At 1.3 or 1.5 wt % cross-linker concentration, the linear rheological markers (G^* and tan δ, Figure 10a,b) feature a piece-wise evolution, respectively increasing and decreasing by a factor close to 2 between 40 and 60 vol % slime, then saturating beyond 60 vol % slime. The trends for the critical strain and stress (Figure 10c,d) are less clear. One sample (1.5 wt % cross-linker, red circles) seems to feature a monotonic (yet faster below 60 vol % slime than above) decrease in both γ_c and σ_c. In the other one (1.3 wt % cross-linker, black squares), γ_c and σ_c decrease abruptly by more than 1 order of magnitude between 40 and 60 vol % slime, and then gradually increase up to intermediate values. Finally, at higher cross-linker concentration (2.0 wt %, blue triangles), where the gel is essentially not dissipative, slime dilution shows no effect on the gel rheology.

Diluting the snail slime therefore adds another possible, yet limited, degree of freedom to adjust the rheological properties of slime gels. Provided that the concentration of cross-linker is low enough, the viscoelasticity can be slightly reduced, and the damping ratio, critical strain, and critical stress can be increased. For instance, the rheological properties of the 1.3 wt % PEG-4SH gel prepared with 40 vol % slime all lie within the expected range of human sputum. In summary, slime dilution is rather limited to fine-tuning the properties of snail-slime-based gels, mostly driven by the cross-linker concentration, but can help make them more dissipative and thereby widen the window in which they can be used as mucus models.

The rheological results presented in Figures 8 and 10, together with the cross-linking scheme proposed in Figure 2b,c, allow us to propose a tentative phase diagram of the snail-slime-PEG-4SH system (Figure 11).

As supported by Figure 2, the oligomer molecules can only connect with PEG-4SH by one end and form multimers through disulfide bonds (Figure 3), composed of up to four oligomers branched to one cross-linker. Oligomers, as well as multimers, can also interact reversibly with each other, but a cohesive gel structure can only form when multimers are sufficiently close to form a percolating network. In other words, oligomers, cross-linker molecules, or associations of one single oligomer to a cross-linker molecule cannot contribute to the gel formation. Forming a gel thus requires both slime and cross-linker concentrations to be sufficient.

Let us first assume either slime or cross-linker concentration is low. In this dispersed regime, multimers remain scarce, so that the mean distance between multimers, $\langle d \rangle$, is much larger than their typical gyration diameter, D. The system is thus a solution of isolated multimers, possibly with excess free cross-linker molecules or oligomers. This regime was experimentally observed below ~40 vol % slime or below ~0.6 wt % with nominal slime.

https://doi.org/10.1021/acs.biomac.3c01043
Biomacromolecules 2024, 25, 400−412

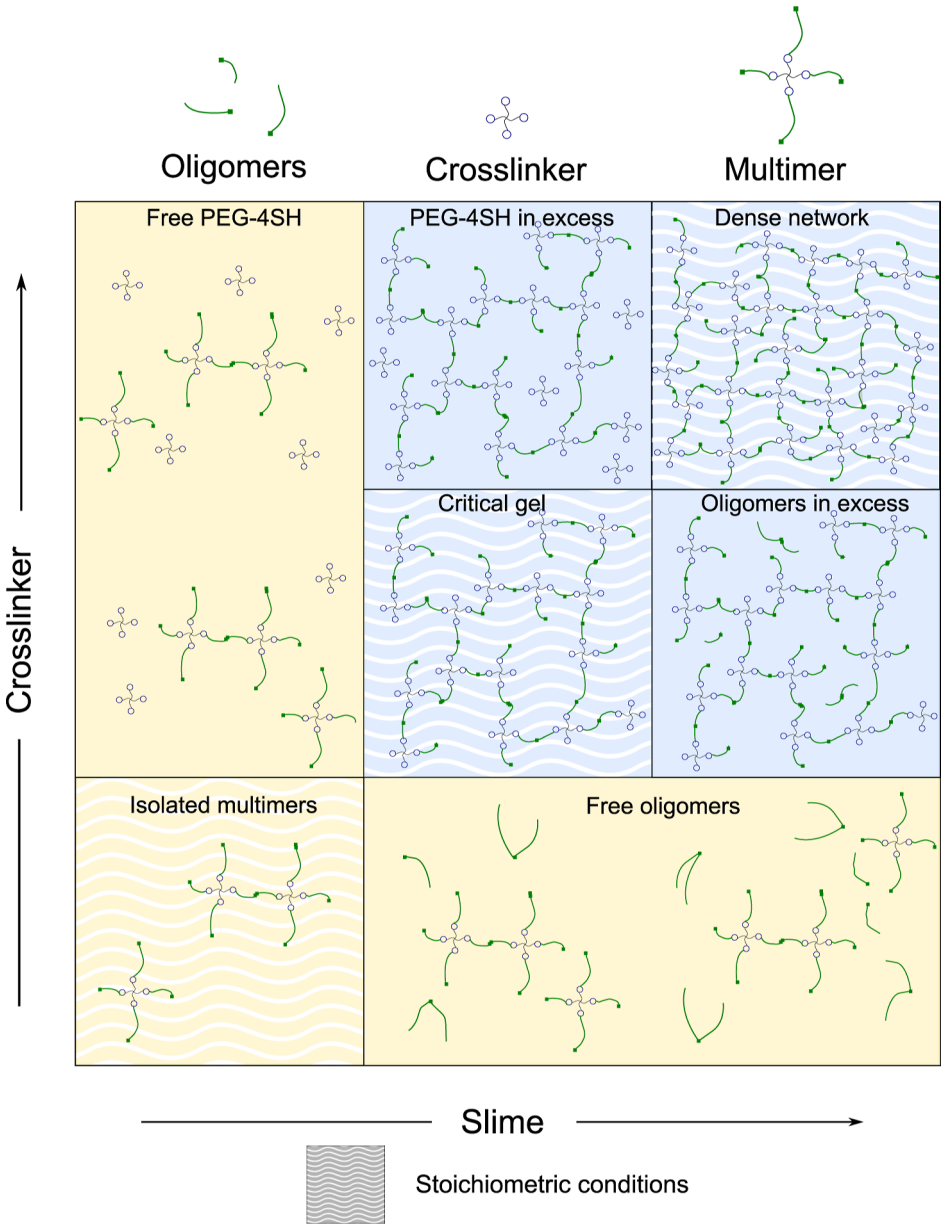

Figure 11. Schematic phase diagram of the slime-cross-linker system, based on the assumption that the network builds upon a combination of disulfide bonds (through PEG cross-linking) and reversible interactions (through slime−slime interactions). Cross-linker and oligomer molecules are represented as in Figure 2, the site for oligomer−oligomer reversible interaction is denoted by the bullet. The yellow and blue areas correspond to viscous liquid and gel phases, respectively. The squares with the wavy background represent stoichiometric conditions.

When both the slime and cross-linker concentrations are sufficient, viz. when $\langle d \rangle \leq D$, multimers interact reversibly with each other over a large scale. A cohesive gel forms, whose yield stress is given by the reversible interactions between multimers. Out of the stoichiometric conditions, free oligomers or cross-linker molecules also persist. As long as oligomers remain available, adding more PEG-4SH can increase the density of cross-links and thereby reinforce the gel. The rheological properties of the gel are thus adjustable through cross-linker concentration, as observed with fully concentrated slime between ∼0.6 and ∼2.5−3 wt % (Figure 8), corresponding respectively to the critical and stoichiometric concentrations in the native slime solution. Beyond c_s, PEG-4SH becomes in excess, and adding more does not affect the gel rheology.

The evolution with slime concentration is similar: adding oligomers densifies the gel until stoichiometry is reached. The rheological properties of the gel are then fixed, as observed in the 1.3 and 1.5 wt % PEG-4SH cases in Figure 10. However, the rheological constancy of the 2.0 wt % PEG-4SH gel above 40 vol % slime cannot be interpreted under this scheme.

CONCLUSION

In the present paper, we formulate and characterize a new biobased gel designed as a possible airway mucus model with tunable rheological properties. This gel, based on snail-slime cross-linked with four-arm thiol PEG molecule, can be reproducibly prepared with commercial components. The addition of synthetic cross-linker was needed as the macromolecules found in snail slime are very small (<10 kDa) and therefore not able to self-assemble in a 3D network. Results from SDS-PAGE chromatograms suggest that the oligomer molecules found in pure slime can only connect to one cross-

https://doi.org/10.1021/acs.biomac.3c01043
Biomacromolecules 2024, 25, 400−412

linker molecule, and interact reversibly with each other. Beyond a critical cross-linker concentration c_0, a gel network builds up, resulting from covalent disulfide bonds as verified by using NAC disulfide bonds disruptor, and reversible interactions between multimers. Although these gels are structurally distinct from mucus, the disulfide bonding covalent association between mucins is reproduced.

The macrorheological properties of these gels can be tuned by changing the cross-linker (and, to a lower extent, slime) concentration, displaying values of linear viscoelasticity, damping ratio, critical strain and critical stress that can all be, separately or together, quantitatively comparable to the values reported with pathological sputum (CF and NCFB).[24] Especially, although snail-slime-based gels are, in general, weakly dissipative, they can become comparable to sputum in a narrow concentration window. However, at the microscale, more research efforts are needed to understand if a correlation exists between the heterogeneous diffusive behavior observed in our mucus model and in sputa by passive microrheology, and the mechanical response observed in oscillatory rheometry (i.e., G'' overshoot).

To support the application potential of snail-slime-based gels as models of respiratory mucus, future research directions could include comprehensive studies of reducing agents, biocompatibility with epithelial cells, and the ability to grow bacterial colonies.

■ ASSOCIATED CONTENT

Supporting Information

The Supporting Information is available free of charge at https://pubs.acs.org/doi/10.1021/acs.biomac.3c01043.

> Gelation time of snail-slime-based hydrogel followed by the evolution of complex modulus G^* obtained from rotational rheometry, oscillatory strain sweep comparison for snail-slime-based hydrogel at different imposed temperatures, and prepared from different batches of snail slime, and Herschel−Bulkley model fitting parameters for flow curves experimental data (PDF)

■ AUTHOR INFORMATION

Corresponding Author

Hugues Bodiguel − *Univ. Grenoble Alpes, CNRS, 38000 Grenoble, France;* orcid.org/0000-0003-2348-6966; Email: hugues.bodiguel@univ-grenoble-alpes.fr

Authors

Diego Milian − *Univ. Grenoble Alpes, CNRS, 38000 Grenoble, France; Rheonova, 38610 Gières, France;* orcid.org/0000-0002-1798-2384

Matthieu Robert de Saint Vincent − *Univ. Grenoble Alpes, CNRS, 38000 Grenoble, France; Rheonova, 38610 Gières, France*

Jérémy Patarin − *Rheonova, 38610 Gières, France*

Complete contact information is available at: https://pubs.acs.org/10.1021/acs.biomac.3c01043

Funding

LRP is part of the LabEx Tec 21 (Investissements d'Avenir−grant agreement ANR-11-LABX-0030) and Institut Carnot PolyNat (Investissements d'Avenir−grant agreement ANR-11-CARN-030−01). This project is also part of ANR Mucus, grant agreement ANR-18-LCV2−0005.

Notes

The authors declare no competing financial interest.

■ ACKNOWLEDGMENTS

The authors acknowledge Lydia Esteban Enjuto for the collection and preparation of native sputum samples, and Mai Duong for her help with the SDS-PAGE test and insightful discussions.

■ REFERENCES

(1) Boucher, R. C. Muco-Obstructive Lung Diseases. *N. Engl. J. Med.* **2019**, *380*, 1941−1953.

(2) Fass, D.; Thornton, D. J. Mucin networks: Dynamic structural assemblies controlling mucus function. *Curr. Opin. Struct. Biol.* **2023**, *79*, 102524.

(3) Loiseau, E.; Gsell, S.; Nommick, A.; Jomard, C.; Gras, D.; Chanez, P.; D'Ortona, U.; Kodjabachian, L.; Favier, J.; Viallat, A. Active mucus−cilia hydrodynamic coupling drives self-organization of human bronchial epithelium. *Nat. Phys.* **2020**, *16*, 1158−1164.

(4) Mesdjian, O.; Wang, C.; Gsell, S.; D'Ortona, U.; Favier, J.; Viallat, A.; Loiseau, E. Longitudinal to Transverse Metachronal Wave Transitions in an in Vitro Model of Ciliated Bronchial Epithelium. *Phys. Rev. Lett.* **2022**, *129*, 038101.

(5) Mauroy, B.; Flaud, P.; Pelca, D.; Fausser, C.; Merckx, J.; Mitchell, B. R. Toward the modeling of mucus draining from human lung: Role of airways deformation on air-mucus interaction. *Front. physiol.* **2015**, *6*, 145796.

(6) Chateau, S.; D'Ortona, U.; Poncet, S.; Favier, J. Transport and mixing induced by beating cilia in human airways. *Front. physiol.* **2018**, *9*, 161.

(7) Galko, A.; Gsell, S.; D'Ortona, U.; Morin, L.; Favier, J. Pulsated Herschel-Bulkley flows in two-dimensional channels: A model for mucus clearance devices. *Phys. Rev. Fluids* **2022**, *7*, 053301.

(8) Stilma, W.; Lilien, T. A.; Bos, L. D.; Saatpoor, A.; Elsayed, O.; Paulus, F.; Schultz, M. J.; Bem, R. A.; Linssen, R. S. Airway Mucus in Invasively Ventilated Critically Ill Patients: Comparing Rheology to a Clinical Classification System. *Respir. Care* **2023**, *68*, 10628.

(9) Tomaiuolo, G.; Rusciano, G.; Caserta, S.; Carciati, A.; Carnovale, V.; Abete, P.; Sasso, A.; Guido, S. A new method to improve the clinical evaluation of cystic fibrosis patients by mucus viscoelastic properties. *PLoS One* **2014**, *9*, No. e82297.

(10) Volpato, M.; Vialaret, J.; Hirtz, C.; Petit, A.; Suehs, C.; Patarin, J.; Matzner-Lober, E.; Vachier, I.; Molinari, N.; Bourdin, A.; Charriot, J. Rheology predicts sputum eosinophilia in patients with muco-obstructive lung diseases. *Biochem. Biophys. Res. Commun.* **2022**, *622*, 64−71.

(11) Schömig, V. J.; Käsdorf, B. T.; Scholz, C.; Bidmon, K.; Lieleg, O.; Berensmeier, S. An optimized purification process for porcine gastric mucin with preservation of its native functional properties. *RSC Adv.* **2016**, *6*, 44932−44943.

(12) Marczynski, M.; Winkeljann, B.; Lieleg, O. *Biopolymers for Biomedical and Biotechnological Applications*; John Wiley & Sons, Ltd, 2021; Chapter 6, pp 181−208.

(13) Madsen, J. B.; Pakkanen, K. I.; Duelund, L.; Svensson, B.; Hachem, M. A.; Lee, S. A simplified chromatographic approach to purify commercially available bovine submaxillary mucins (BSM). *Prep. Biochem. Biotechnol.* **2015**, *45*, 84−99.

(14) Sharma, A.; Kwak, J. G.; Kolewe, K. W.; Schiffman, J. D.; Forbes, N. S.; Lee, J. In Vitro Reconstitution of an Intestinal Mucus Layer Shows That Cations and pH Control the Pore Structure That Regulates Its Permeability and Barrier Function. *ACS Appl. Bio Mater.* **2020**, *3*, 2897−2909.

(15) Celli, J. P.; Turner, B. S.; Afdhal, N. H.; Ewoldt, R. H.; McKinley, G. H.; Bansil, R.; Erramilli, S. Rheology of gastric mucin exhibits a pH-dependent sol-gel transition. *Biomacromolecules* **2007**, *8*, 1580−1586.

(16) Marczynski, M.; Jiang, K.; Blakeley, M.; Srivastava, V.; Vilaplana, F.; Crouzier, T.; Lieleg, O. Structural Alterations of Mucins

Are Associated with Losses in Functionality. *Biomacromolecules* **2021**, *22*, 1600−1613.
(17) Abodinar, A.; Tømmeraas, K.; Ronander, E.; Smith, A. M.; Morris, G. A. The physicochemical characterisation of pepsin degraded pig gastric mucin. *Int. J. Biol. Macromol.* **2016**, *87*, 281−286.
(18) Kočevar-Nared, J.; Kristl, J.; Šmid-Korbar, J. Comparative rheological investigation of crude gastric mucin and natural gastric mucus. *Biomaterials* **1997**, *18*, 677−681.
(19) Joyner, K.; Song, D.; Hawkins, R. F.; Silcott, R. D.; Duncan, G. A. A rational approach to form disulfide linked mucin hydrogels. *Soft Matter* **2019**, *15*, 9632−9639.
(20) Song, D.; Iverson, E.; Kaler, L.; Bader, S.; Scull, M. A.; Duncan, G. A. Modeling Airway Dysfunction in Asthma Using Synthetic Mucus Biomaterials. *ACS Biomater. Sci. Eng.* **2021**, *7*, 2723−2733.
(21) Roberts, G. P. The role of disulfide bonds in maintaining the gel structure of bronchial mucus. *Arch. Biochem. Biophys.* **1976**, *173*, 528−537.
(22) Wagner, C. E.; Wheeler, K. M.; Ribbeck, K. Mucins and Their Role in Shaping the Functions of Mucus Barriers. *Annu. Rev. Cell Dev. Biol.* **2018**, *34*, 189−215.
(23) Patarin, J.; Ghiringhelli, E.; Darsy, G.; Obamba, M.; Bochu, P.; Camara, B.; Quétant, S.; Cracowski, J. L.; Cracowski, C.; Robert de Saint Vincent, M. Rheological analysis of sputum from patients with chronic bronchial diseases. *Sci. Rep.* **2020**, *10*, 15685.
(24) Esteban Enjuto, L.; Robert de Saint Vincent, M.; Maurin, M.; Degano, B.; Bodiguel, H. Sputum handling for rheology. *Sci. Rep.* **2023**, *13*, 7695.
(25) Daniele, M. A.; Adams, A. A.; Naciri, J.; North, S. H.; Ligler, F. S. Interpenetrating networks based on gelatin methacrylamide and PEG formed using concurrent thiol click chemistries for hydrogel tissue engineering scaffolds. *Biomaterials* **2014**, *35*, 1845−1856.
(26) Wang, J.; Youngblood, R.; Cassinotti, L.; Skoumal, M.; Corfas, G.; Shea, L. An injectable PEG hydrogel controlling neurotrophin-3 release by affinity peptides. *J. Controlled Release* **2021**, *330*, 575−586.
(27) Yuan, J.; Maturavongsadit, P.; Metavarayuth, K.; Luckanagul, J. A.; Wang, Q. Enhanced Bone Defect Repair by Polymeric Substitute Fillers of MultiArm Polyethylene Glycol-Crosslinked Hyaluronic Acid Hydrogels. *Macromol. Biosci.* **2019**, *19*, 1900021.
(28) Park, J.; Lee, S.; Lee, M.; Kim, H. S.; Lee, J. Y. Injectable Conductive Hydrogels with Tunable Degradability as Novel Implantable Bioelectrodes. *Small* **2023**, *19*, 2300250.
(29) Pacheco, D. P.; Butnarasu, C. S.; Briatico Vangosa, F.; Pastorino, L.; Visai, L.; Visentin, S.; Petrini, P. Disassembling the complexity of mucus barriers to develop a fast screening tool for early drug discovery. *J. Mater. Chem. B* **2019**, *7*, 4940−4952.
(30) Butnarasu, C.; Caron, G.; Pacheco, D. P.; Petrini, P.; Visentin, S. Cystic Fibrosis Mucus Model to Design More Efficient Drug Therapies. *Mol. Pharmaceutics* **2022**, *19*, 520−531.
(31) Huck, B. C.; Hartwig, O.; Biehl, A.; Schwarzkopf, K.; Wagner, C.; Loretz, B.; Murgia, X.; Lehr, C. M. Macro- And Microrheological Properties of Mucus Surrogates in Comparison to Native Intestinal and Pulmonary Mucus. *Biomacromolecules* **2019**, *20*, 3504−3512.
(32) Anwarul Hasan, M. D.; Lange, C. F.; King, M. L. Effect of artificial mucus properties on the characteristics of airborne bioaerosol droplets generated during simulated coughing. *J. Non-Newtonian Fluid Mech.* **2010**, *165*, 1431−1441.
(33) Nelson, A. Z.; Ewoldt, R. H. Design of yield-stress fluids: A rheology-to-structure inverse problem. *Soft Matter* **2017**, *13*, 7578−7594.
(34) Piau, J. M. Carbopol gels: Elastoviscoplastic and slippery glasses made of individual swollen sponges. *J. Non-Newtonian Fluid Mech.* **2007**, *144*, 1−29.
(35) Dinkgreve, M.; Paredes, J.; Denn, M. M.; Bonn, D. On different ways of measuring "the" yield stress. *J. Non-Newtonian Fluid Mech.* **2016**, *238*, 233−241.
(36) Button, B.; Goodell, H. P.; Atieh, E.; Chen, Y.-C.; Williams, R.; Shenoy, S.; Lackey, E.; Shenkute, N. T.; Cai, L.-H.; Dennis, R. G.; Boucher, R. C.; Rubinstein, M. Roles of mucus adhesion and cohesion in cough clearance. *Proc. Natl. Acad. Sci. U.S.A.* **2018**, *115*, 12501−12506.
(37) Dubaissi, E.; Rousseau, K.; Hughes, G. W.; Ridley, C.; Grencis, R. K.; Roberts, I. S.; Thornton, D. J. Functional characterization of the mucus barrier on the Xenopus tropicalis skin surface. *Proc. Natl. Acad. Sci. U.S.A.* **2018**, *115*, 726−731.
(38) Ewoldt, R. H.; Clasen, C.; Hosoi, A. E.; McKinley, G. H. Rheological fingerprinting of gastropod pedal mucus and synthetic complex fluids for biomimicking adhesive locomotion. *Soft Matter* **2007**, *3*, 634−643.
(39) Böni, L. J.; Zurflüh, R.; Baumgartner, M. E.; Windhab, E. J.; Fischer, P.; Kuster, S.; Rühs, P. A. Effect of ionic strength and seawater cations on hagfish slime formation. *Sci. Rep.* **2018**, *8*, 9867.
(40) Ballance, S.; Howard, M.; White, K. N.; McCrohan, C. R.; Thornton, D. J.; Sheehan, J. K. Partial characterisation of high-molecular weight glycoconjugates in the trail mucus of the freshwater pond snail Lymnaea stagnalis. *Comp. Biochem. Physiol., Part B: Biochem. Mol. Biol.* **2004**, *137*, 475−486.
(41) Cerullo, A. R.; McDermott, M. B.; Pepi, L. E.; Liu, Z. L.; Barry, D.; Zhang, S.; Yang, X.; Chen, X.; Azadi, P.; Holford, M.; Braunschweig, A. B. Comparative mucomic analysis of three functionally distinct Cornu aspersum Secretions. *Nat. Commun.* **2023**, *14*, 5361.
(42) Ricci, A.; Gallorini, M.; Feghali, N.; Sampò, S.; Cataldi, A.; Zara, S. Snail Slime Extracted by a Cruelty Free Method Preserves Viability and Controls Inflammation Occurrence: A Focus on Fibroblasts. *Molecules* **2023**, *28*, 1222.
(43) Zhong, T.; Min, L.; Wang, Z.; Zhang, F.; Zuo, B. Controlled self-assembly of glycoprotein complex in snail mucus from lubricating liquid to elastic fiber. *RSC Adv.* **2018**, *8*, 13806−13812.
(44) Dhiman, V.; Pant, D. Human health and snails. *J. Immunoassay Immunochem.* **2021**, *42*, 211−235.
(45) Cristiano, L.; Guagni, M. Zooceuticals and Cosmetic Ingredients Derived from Animals. *Cosmetics* **2022**, *9*, 13.
(46) Ewoldt, R. H.; Hosoi, A. E.; McKinley, G. H. Nonlinear viscoelastic biomaterials: Meaningful characterization and engineering inspiration. *Integr. Comp. Biol.* **2009**, *49*, 40−50.
(47) Fukui, Y.; Fukuda, M.; Fujimoto, K. Generation of mucin gel particles with self-degradable and -releasable properties. *J. Mater. Chem. B* **2018**, *6*, 781−788.
(48) Lamont, J. T.; Ventola, A. S.; Trotman, B. W.; Soloway, R. D. Mucin Glycoprotein Content of Human Pigment Gallstones. *Hepatology* **1983**, *3*, 377−382.
(49) Nelson, A. Z.; Schweizer, K. S.; Rauzan, B. M.; Nuzzo, R. G.; Vermant, J.; Ewoldt, R. H. Designing and transforming yield-stress fluids. *Curr. Opin. Solid State Mater. Sci.* **2019**, *23*, 100758.
(50) Sevier, C. S.; Kaiser, C. A. Formation and transfer of disulphide bonds in living cells. *Nat. Rev. Mol. Cell Biol.* **2002**, *3*, 836−847.
(51) Samuni, Y.; Goldstein, S.; Dean, O. M.; Berk, M. The chemistry and biological activities of N-acetylcysteine. *Biochim. Biophys. Acta* **2013**, *1830*, 4117−4129.
(52) Hyun, K.; Kim, S. H.; Ahn, K. H.; Lee, S. J. Large amplitude oscillatory shear as a way to classify the complex fluids. *J. Non-Newtonian Fluid Mech.* **2002**, *107*, 51−65.
(53) Donley, G. J.; Singh, P. K.; Shetty, A.; Rogers, S. A. Elucidating the G" overshoot in soft materials with a yield transition via a time-resolved experimental strain decomposition. *Proc. Natl. Acad. Sci. U.S.A.* **2020**, *117*, 21945−21952.
(54) Larson, R. The Structure and Rheology of Complex Fluids. *Topics in Chemical Engineering*; OUP: USA, 1999.
(55) Martin, J. E.; Adolf, D.; Wilcoxon, J. P. Viscoelasticity near the sol-gel transition. *Phys. Rev. A* **1989**, *39*, 1325−1332.
(56) De Gennes, P.-G. *Scaling Concepts in Polymer Physics*; Cornell university press, 1979.
(57) Guo, L.; Colby, R. H.; Lusignan, C. P.; Howe, A. M. Physical gelation of gelatin studied with rheo-optics. *Macromolecules* **2003**, *36*, 10009−10020.

https://doi.org/10.1021/acs.biomac.3c01043
Biomacromolecules 2024, 25, 400−412

(58) Cho, J.; Heuzey, M.-C. Dynamic scaling for gelation of a thermosensitive chitosan-β-glycerophosphate hydrogel. *Colloid Polym. Sci.* **2008**, *286*, 427−434.
(59) Tordjeman, P.; Fargette, C.; Mutin, P. Viscoelastic properties of a cross-linked polysiloxane near the sol−gel transition. *J. Rheol.* **2001**, *45*, 995−1006.
(60) Moura, M. J.; Figueiredo, M. M.; Gil, M. H. Rheological study of genipin cross-linked chitosan hydrogels. *Biomacromolecules* **2007**, *8*, 3823−3829.
(61) Weissenberg, K. A continuum theory of rheological phenomena. *Nature* **1947**, *159*, 310−311.

https://doi.org/10.1021/acs.biomac.3c01043
Biomacromolecules 2024, 25, 400−412